Ground and Excited State Properties and Vibronic Coupling Analysis of the Creutz−Taube Ion, $[(NH_3)_5Ru\text{-pyrazine-}Ru(NH_3)_5]^{5+}$, Using DFT

Alessandro Bencini,* Ilaria Ciofini, Claude A. Daul, and Alessandro Ferretti

Contribution from the Dipartimento di Chimica, Università di Firenze, I-50144 Firenze, Italy, Institut de Chimie Inorganique et Analitique, Université de Fribourg, CH-1700 Fribourg, Switzerland, and Istituto di Chimica Quantistica ed Energetica Molecolare, C.N.R., I-56126 Pisa, Italy

Received June 15, 1999

Abstract: In this paper we analyze using Density Functional Theory (DFT) the electronic structure of the Creutz−Taube ion, $[(NH_3)_5Ru\text{-pyrazine-}Ru(NH_3)_5]^{5+}$, a classical example of a mixed-valence complex. A complete structural and bonding analysis, description of the low-lying excited states, and a vibronic coupling calculation along both the symmetric and the antisymmetric Ru-pyrazine-Ru stretching mode are presented. The results are in very good agreement with the reported experimental data and we are able to assign unambiguously this compound as a Class III system, following the Robin and Day classification. In this work we demonstrate that DFT does offer a unique tool for handling the localization−delocalization of electrons in mixed-valence systems and therefore we expect that this approach can play an important role in characterizing electron-transfer systems. Localized Ru−N(pyrazine) stretching in the range 254−275 cm^{-1} has been estimated from our calculations, which should be used in future model Hamiltonians which aim to include the Ru−pyz bond vibration to describe the spectral features of the Creutz−Taube ion.

Introduction

Beginning with the work by Creutz and Taube,[1] the study of polynuclear compounds made by metal centers, formally in different oxidation states, intercalated by organic bridging ligands opened new fields of research: the chemistry and physics of *mixed-valence* compounds. These compounds are perfect candidates for the study of intramolecular electron and energy transfer,[2] in both homonuclear and heteronuclear systems. Furthermore, since mixed-valence compounds can be conductive,[3] as well as exhibit significant nonlinear optical[4] and magnetic properties,[5,6] they are also of interest for a possible application in molecular electronics.

For the reasons above, there is still intense activity in the field and, to date, a large variety of mixed-valence compounds have been synthesized and their properties are currently being studied. Rather comprehensive reviews have been written by Creutz[7] and Crutchley.[8] Recent contributions to be mentioned here are those by Olabe et al.[9] for Os, Fe, and Ru complexes, by Crutchley et al.,[10] and by Lin et al.[11]

The pyrazine-bridged Ru dimer, $[(NH_3)_5Ru\text{-pyz-}Ru(NH_3)_5]^{+5}$, also known as the Creutz−Taube ion, can be considered as one of the classical examples of this class of systems. It formally contains a Ru(II)−Ru(III) pair. In the last years, much attention has been devoted to its near-IR−vis optical properties, in view of understanding whether the compound is delocalized or not, and estimating the through-bridge metal−metal interaction.[12−14] In this perspective, several theoretical models have been developed,[3b,15−23] with the aim of interpreting the experimental findings and thus underlying the main physics involved in the electron-delocalization process. Furthermore, electroabsorption (Stark effect) measurements, such as those reported for the first time by Oh, Sano, and Boxer,[24] and further developed by the

* Address correspondence to this author at Università di Firenze.

(1) Creutz, C.; Taube, H. *J. Am. Chem. Soc*. **1969**, *91*, 3988.
(2) Balzani, V.; Scandola, F. *Supramolecular Photochemistry*; Horwood: Chichester, U.K., 1991.
(3) (a) Hanack, M.; Lang, M. *Adv. Mater.* **1994**, *6*, 819. (b) Ferretti, A.; Lami, A. *Chem. Phys.* **1994**, *181*, 107. Ferretti, A.; Lami, A. *Chem. Phys. Lett.* **1994**, *220*, 327.
(4) Ferretti, A.; Lami, A.; Villani, G. *J. Phys. Chem.* **1997**, *101*, 9439.
(5) (a) Bencini, A.; Palii, A. V.; Ostrovsky, S. O.; Tsukerblat, B. S.; Uytterhoeven, M. G. *Mol. Phys.* **1995**, *86*, 1085. (b) Bominaar, E. L.; Achim, C.; Borshch, S. A.; Gired, J.-J.; Münck, E. *Inorg. Chem.* **1997**, *36*, 3689. (c) Borrás-Almenar, J. J.; Coronado, E.; Ostrovsky, S. M.; Palii, A. V.; Tsukerblat, B. S. *Chem. Phys. Lett.* **1999**, *240*, 149. (d) Belinsky M. I. *Chem. Phys. Lett.* **1999**, *240*, 303.
(6) Barone, V.; Bencini, A.; Ciofini, I.; Daul, C. A.; Totti, F. *J. Am. Chem. Soc.* **1998**, *120*, 8357.
(7) Creutz, C. *Prog. Inorg. Chem.* **1983**, *30*, 1.
(8) Crutchley, R. J. *Adv. Inorg. Chem.* **1994**, *41*, 273.
(9) (a) Almaraz, A. E.; Gentil, L. A.; Baraldo, L. M.; Olabe, J. A. *Inorg. Chem.* **1996**, *35*, 7718. (b) Almaraz, A. E.; Gentil, L. A.; Baraldo, L. M.; Olabe. J, A. *Inorg. Chem.* **1997**, *36*, 1517. (c) Hornung, M. F.; Bauman, F.; Kaim, W.; Olabe, J. A.; Slep, L. D.; Fiedler, J. *Inorg. Chem.* **1998**, *37*, 311.
(10) 0) (a) Rezvani, A. R.; Bensimon, C.; Cromp, B.; Reber, C.; Greedan, J. E.; Kondratiev, V. V.; Crutchley, R. J. *Inorg. Chem.* **1997**, *36*, 3322. (b) Nacklicki, M. L.; White, C. A.; Plante, L. L.; Evans, C. E. B.; Crutchley, R. J. *Inorg. Chem.* **1998**, *37*, 1880.
(11) Lin, C.-L.; Hung, K.; Yeh, A.; Tsen, H.-T.; Su, C.-C. *Inorg. Chem.* **1999**, *38*, 411.
(12) Oh, D. H.; Boxer, S. G. *J. Am. Chem. Soc.* **1990**, *112*, 8161.
(13) (a) Petrov, V.; Hupp, J. T.; Mottley, C.; Mann, L. C. *J. Am. Chem. Soc.* **1994**, *116*, 2171. (b) Lu, H.; Petrov, V.; Hupp, J. T. *Chem. Phys. Lett.* **1995**, *235*, 521.
(14) Hupp, J. T.; Dong, Y. *Inorg. Chem.* **1994**, *33*, 4421.
(15) Hush, N. S. *Prog. Inorg. Chem.* **1967**, *8*, 391.
(16) Piepho, S. B.; Krausz, E. R.; Schatz, P. N. *J. Am. Chem. Soc.* **1978**, *100*, 2996.
(17) Piepho, S. B. *J. Am. Chem. Soc.* **1988**, *110*, 6319. Piepho, S. B. *J. Am. Chem. Soc.* **1990**, *112*, 4197.
(18) Zhang, L.-T.; Ko, J.; Ondrechen, M. J. *J. Am. Chem. Soc.* **1987**, *109*, 1666.
(19) Ondrechen, M. J.; Ko, J.; Zhang, L.-T. *J. Am. Chem. Soc.* **1987**, *109*, 1672.
(20) Cave, R. J.; Newton, M. D. *Chem. Phys. Lett.* **1996**, *249*, 15.

10.1021/ja9920258 CCC: $18.00
Published on Web 11/30/1999

Brookhaven group[25] and by Hupp et al.,[26] through a deeper investigation of the bands in the near-IR−vis, in terms of an expansion in the static field of the transition dipole moment, allow the distinction to be made if the system is or is not delocalized.[27] Stark spectra could also be simulated by theoretical methods, which must be able to account for not only position and intensity of the bands but also their line shape profile. In fact, since the observed difference spectra[24−26] originate by both displacement and enlargement (or narrowing) of the bands, due to the static electric field applied, they can be correctly predicted only if the line shape profile is also well reproduced. To date, this can be accomplished only by means of suitable model Hamiltonians,[27,28] which must then contain a good description of the electronic terms,[3b,22] as well as of both the contribution of nuclear degrees of freedom and vibronic coupling.[16,17,19,21,23] From a computational point of view, the size of the Creutz−Taube ion is so large that sophisticated post-HF treatments (as for example configuration interaction, CI) of the whole ground and excited potential energy surfaces are unfeasible. As a matter of fact, CI calculations have been performed only on the monomer compounds $[(NH_3)_5Ru\text{-}pyz]^{m+}$ ($m = 2, 3$; pyz = pyrazine)[29] and $[(NH_3)_5Ru(4,4'\text{-}bpy)]^{+2}$ (bpy = bipyridine)[30] to assign their solution absorption spectra.

In this context density functional theory (DFT) appears to be the most suitable approach. In particular, we already applied DFT to study the ground-state potential energy surface of mixed-valence complexes with both localized[31] and delocalized[6] valence electrons. Due to good agreement with the experimental information, we decided to apply the same formalism to describe the ground state electronic structure of the most well-known mixed-valence complex: the Creutz−Taube ion. A detailed bonding and structural analysis was performed for the ground state by using both local and nonlocal functionals. The relevant electronic excitations were computed and compared to the experimental values. These results were found substantially in agreement with previous Xα-DVM calculations.[18] The analysis of the ground-state potential energy surface (PES) along the Ru−pyz distance confirms the delocalized nature of the complex by the presence of a single minimum with a *quasi*-parabolic shape. The computed PES was also used to estimate the frequency of the Ru−pyz stretch, which plays a significant role in the Ru−Ru electron-transfer process and is therefore also important when building vibronic model Hamiltonians.

Computational Details

All the calculations have been performed using the Amsterdam Density Functional (ADF) program package.[32] Either local density (LDA) or generalized gradient approximation (GGA) for exchange-correlation functionals was used in the calculations. LDA was applied with the Xα functional for the exchange[33] and the Vosko, Wilk, and Nusair functional[34] for the correlation potential. When explicitly specified, the Stoll[35] correlation correction was applied to the VWN functional. GGA was applied by using the Becke88[36] exchange and the Perdew86[37] correlation (BP), and the Perdew-Wang91[38] exchange-correlation functional (PW91). Several calculations were performed also including the scalar relativistic corrections, Darwin, and mass-velocity, in the *quasi*-relativistic approach[39] as implemented in ADF.

The frozen core (FC) approximation for the inner core electrons was used for all atoms. The orbitals up to 3d for Ru, and 1s for N and C atoms were kept frozen. Valence electrons of non-metallic atoms were treated with double-ζ basis functions except hydrogens which were treated with a single-ζ function. For carbon and nitrogen atoms a single-ζ d polarization function was added to the valence basis set. Exponents of the Slater functions given with the ADF2.3 distribution were used. Valence electrons of Ru were treated with triple-ζ basis functions except the 4s orbital which was expanded in a double-ζ basis. A single-ζ 5p polarization function was added. Two different sets of exponents for the STO's were used: the standard one, given in the ADF2.3 atomic database, (**B1**), and a set optimized by fitting the numerically computed Kohn−Sham atomic orbitals[40] for the Ru(II) and the Ru(III) atom (**B2**). The **B2** basis, in the format of an atomic data set for ADF2.3, is available as Supporting Information (Table SI). This basis was used only in these calculations and no extensive test of the quality of the basis has been yet performed.

Electronic transitions were computed by applying the Slater's transition state theory.[33] Geometry optimizations were performed in internal coordinates using the Broyden−Fletcher−Goldfarb−Shanno algorithm[41] to update the Hessian matrix. The N−H bond lengths of the ammonia molecules and the H−N−Ru angles were kept frozen at 1.06 Å and 105°, respectively. The default convergence criteria of ADF2.3 were used except for the precision of the numerical integration which was increased (accint = 6.0). A sketch of the structure of the $[(NH_3)_5Ru(pyz)Ru(NH_3)_5]^{5+}$ cation and the reference system are shown in Figure 1. Complete geometry optimizations were performed imposing a C_{2v} nuclear symmetry, while the analysis of the potential energy surface was performed in C_s, the pyrazine defining the σ plane (xz).

Results and Discussion

For the sake of clarity, this section will be organized into the following subsections: Structural Analysis, Bonding Analysis, Electronic Spectra, and Adiabatic Potential Surfaces.

Structural Analysis. The relevant geometrical parameters obtained by geometry optimization of the $[(NH_3)_5Ru(pyz)Ru(NH_3)_5]^{5+}$ cation are shown in Tables 1 and 2 and compared with the experimental data.[42] Geometries computed with the

(21) Reimers, J. R.; Hush, N. S. *Chem. Phys.* **1996**, *208*, 177.
(22) Ferretti, A.; Lami, A.; Villani, G. *Inorg. Chem.* **1998**, *37*, 2799. Ferretti, A.; Lami, A.; Villani, G. *Inorg. Chem.* **1998**, *37*, 4460.
(23) Ferretti, A.; Lami, A.; Ondrechen, M. J.; Villani, G. *J. Phys. Chem.* **1995**, *99*, 10484; Erratum: **1996**, *100*, 20174.
(24) Oh, D. H.; Sano, M.; Boxer, S. G. *J. Am. Chem. Soc.* **1991**, *113*, 6880.
(25) Shin, Y. K.; Brunschwig, B.; Creutz, C.; Sutin, N. *J. Phys. Chem.* **1996**, *100*, 8157.
(26) Vance, F. W.; Williams, R. D.; Hupp, J. T. *Int. Rev. Phys. Chem.* **1998**, *10*, 247.
(27) (a) Reimers, J. R.; Hush, N. S. *J. Phys. Chem.* **1991**, *95*, 9773. (b) Reimers, J. R.; Hush, N. S. *Chem. Phys.* **1993**, *176*, 407.
(28) (a) Murga, L. F.; Ferretti, A.; Lami, A.; Ondrechen, M. J.; Villani, G. *Inorg. Chem. Commun.* **1998**, *1*, 137. (b) Ferretti, A.; Lami, A.; Murga, L. F.; Shehadi, I. A.; Ondrechen, M. J.; Villani, G. *J. Am. Chem. Soc.* **1999**, *121*, 2594.
(29) Cacelli, I.; Ferretti, A. *J. Chem. Phys.* **1998**, *109*, 8583.
(30) Cacelli, I.; Ferretti, A. *J. Phys. Chem.* **1999**, *103*, 4438.
(31) Bencini, A.; Ciofini, I.; Gatteschi, D.; Mattesini, M.; Totti, F. *J. Mol. Cryst. Liq. Cryst.* In press.
(32) *Amsterdam Density Functional (ADF) revision 2.3*; Scientific Computing and Modelling, Theoretical Chemistry, Vrije Universiteit: Amsterdam, 1997. (a) Baerends, E. J.; Ellis, D. E.; Ros, P. *Chem. Phys.* **1973**, *2*, 42. (b) Boerrigter, P. M.; te Velde, G.; Baerends, E. J. *Int. J. Quantum Chem.* **1988**, *33*, 87. (c) te velde, G.; Baerends, E. J. *J. Comput. Phys.* **1992**, *99*, 84. (d) Fonseca Guerra, C.; Visser, O.; Snijders, J. G.; te Velde, G.; Baerends, E. J. In *Methods and Techniques in Computational Chemistry*; Clementi, E., Corongiu, C., Eds.; STEF: Cagliari, 1995; Chapter 8, p 305.
(33) Slater, J. C. *Quantum Theory of Molecules and Solids*; Vol. 4, Self-Consistent Field for Molecules and Solids; McGraw-Hill: New York, 1974.
(34) Vosko, S. H.; Wilk, L.; Nusair, M. *Can. J. Phys.* **1980**, *58*, 1200.
(35) Stoll, H.; Pavlidov, C. M. E.; Preuss, H. *Theor. Chim. Acta* **1978**, *49*, 143.
(36) Becke, A. D. *Phys. Rev. B* **1988**, *38*, 3098.
(37) Perdew, J. P. *Phys. Rev. B* **1986**, *33*, 8822.
(38) Perdew, J. P.; Chevary, J. A.; Vosko, S. H.; Jackson, K. A.; Pederson, M. R.; Singh, D. J.; Fiolhais, C. *Phys. Rev. B* **1992**, *46*, 6671.
(39) Ziegler, T.; Tschinke, V.; Baerends, E. J. *J. Phys. Chem.* **1989**, *93*, 3050.
(40) XATOM: Atomic DFT program developed by one of us (C.A.D.).
(41) Press, W. H.; Flannery, B. P.; Teukolsky, S. A.; Vetterling, W. T. *Numerical Recipes*; Cambridge University Press: Cambridge, 1989.
(42) Furholz, U.; Burgi, H.B.; Wagner, F. E.; Stebler, A.; Ammeter, J. H.; Krausz, E.; Clark, R. J. H.; Stead, M. J.; Ludi, A. *J. Am. Chem. Soc.* **1984**, *106*, 121.

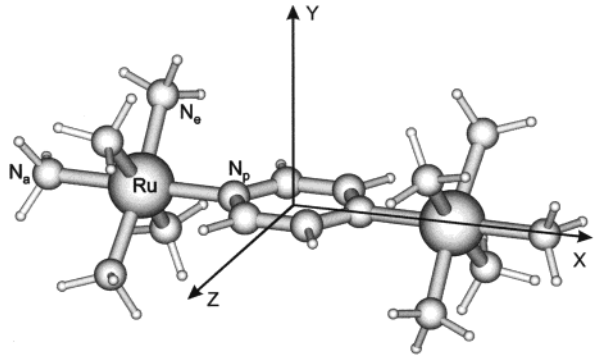

Figure 1. Schematic structure of $[(NH_3)_5Ru(pyz)Ru(NH_3)_5]^{5+}$ and the reference system.

Table 1. Relevant Geometrical Parameters of the $[(NH_3)_5Ru(pyz)Ru(NH_3)_5]^{5+}$ Ion Computed Using **B1**

	nonrelativistic			relativistic			
	LDA/Stoll	PW91	BP	LDA	PW91	BP	exptl[a]
Ru−Ru	7.073	7.292	7.294	6.992	7.161	7.185	6.840/6.877
$Ru-N_p$	2.095	2.204	2.203	2.060	2.127	2.134	1.991
$Ru-N_a$	2.135	2.158	2.162	2.106	2.151	2.154	2.123/2.134
$Ru-N_e$	2.139	2.170	2.176	2.109	2.153	2.159	2.112/2.110
$C-N_p$	1.360	1.358	1.359	1.354	1.365	1.368	1.362/1.364
CC	1.385	1.390	1.391	1.375	1.385	1.387	1.361/1.369
N_pCC	123.4	123.4	123.4	123.6	123.9	124.0	123.3/122.4
CN_pC	113.1	113.2	113.2	112.8	112.2	112.1	114.3

[a] From ref 42.

Table 2. Relevant Geometrical Parameters of the $[(NH_3)_5Ru(pyz)Ru(NH_3)_5]^{5+}$ Ion Computed Using **B2**

	nonrelativistic			relativistic			
	LDA/Stoll	PW91	BP	LDA	PW91	BP	exptl[a]
Ru−Ru	6.786	6.900	6.923	6.703	6.861	6.892	6.840/6.877
$Ru-N_p$	1.966	2.018	2.026	1.927	1.987	1.998	1.991
$Ru-N_a$	2.093	2.112	2.116	2.075	2.109	2.108	2.123/2.134
$Ru-N_e$	2.090	2.116	2.120	2.066	2.105	2.109	2.112/2.110
$C-N_p$	1.362	1.362	1.360	1.357	1.368	1.370	1.362/1.364
CC	1.381	1.384	1.386	1.367	1.380	1.382	1.361/1.369
N_pCC	122.7	122.9	122.9	123.0	123.4	123.5	123.3/122.4
CN_pC	114.5	114.1	114.1	113.9	113.2	112.9	114.3

[a] From ref 42.

B1 and the **B2** basis sets are reported in Tables 1 and 2, respectively. The $Ru-N_p$ distance, reported in Table 1, is overestimated independently of the functional used, and even the introduction of relativistic corrections[39] does not significantly improve the results. It is noteworthy that even the LDA approach, which leads usually to over-bound structures, gives an elongated $Ru-N_p$ bond. This determines the Ru−Ru overall distance to be largely (0.1−0.4 Å) overestimated. On the contrary, the $Ru-NH_3$ and the C−C and C−N bond distances are computed with the usual accuracy of DFT methods. Better geometries were obtained using the **B2** basis, as shown in Table 2. The error on the Ru−N distances is nearly independent of the functional used and in good agreement with the experimental data. The best agreement is achieved using the GGA-relativistic approach. Since the main difference between the bonding character of ammonia and pyrazine is the presence of π interactions in the latter ligand, we think that the metal orbitals optimized in base **B2** can better reproduce this type of interaction. This can be ascribed to the more diffuse character of the 4d functions, which can better overlap with the π system of the bridging pyrazine. Due to the importance of the molecular geometry on the vibronic analysis of the adiabatic ground state, we expect that the (**B2**) basis set will perform better.

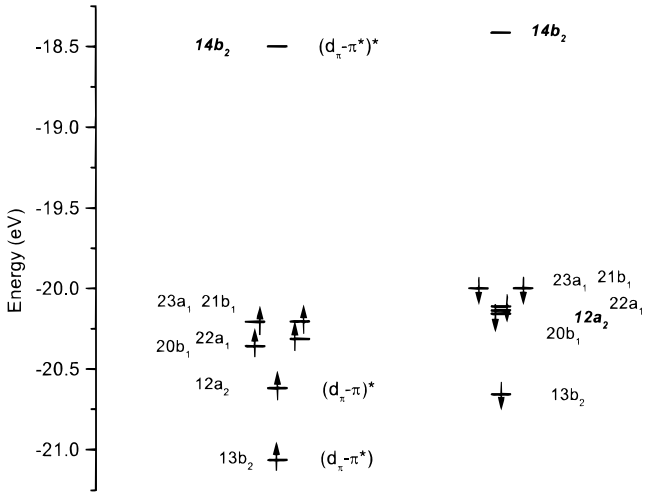

Figure 2. Computed (VWN + Stoll in C_{2v} symmetry) Frontier molecular orbital energy levels for $[(NH_3)_5Ru(pyz)Ru(NH_3)_5]^{5+}$. Up spin orbitals are plotted on the left side, down spin orbitals are plotted on the right side. Empty orbitals are indicated with ***bold italic*** labels.

Bonding Analysis. The charges on the ruthenium atoms computed with the standard Mulliken analysis depend both on the basis set and on the actual form of the functionals. They average to 2.55(5) and 2.07(6) for **B1** and **B2**, respectively. This variation reflects the higher covalency of the Ru−pyrazine bond computed using **B2**. For the sake of simplicity, however, we will continue to call Ru(II) and Ru(III) the two centers. If we neglect the π bonding effects of the pyrazine, the valence 4d electrons of the, formally, Ru(II) and Ru(III) ions lie in the d_π set (t_{2g} in O_h symmetry), and characterize the ligand field low-spin states of the single ions ($^1A_{1g}$ and $^2T_{2g}$ in O_h symmetry). One unpaired electron is expected for the whole system. The d_σ orbitals (e_g in O_h symmetry) are destabilized by the σ antibonding interactions with ammonia and pyrazine and lie, unoccupied, at higher energy. The degeneracy of the six $4d_\pi$ orbitals is removed by the interactions with the π orbitals of the pyrazine. The energies of the frontier orbitals of $[(NH_3)_5Ru(pyz)Ru(NH_3)_5]^{5+}$, computed with (**B1**) at the LDA level (VWN + Stoll), are sketched in Figure 2, and the relevant bonding interactions are shown in Figure 3. The orbital interaction that mostly influences the six $4d_\pi$ orbitals is the π-back-donation between the *"in phase"* combination of the d_{xy} Ru orbitals (see Figure 1 for the labeling of the reference system) and the π^* system of pyrazine. This interaction originates from the doubly occupied bonding orbital, $13b_2$ (Figure 3a), briefly called ($d_\pi-\pi^*$), and the corresponding antibonding orbital $14b_2$ (Figure 3c), $(d_\pi-\pi^*)^*$, which is the LUMO. The unpaired electron is located in the $12a_2$ ($(d_\pi-\pi)^*$) orbital (Figure 3b), which corresponds to the antibonding interaction between the *"out-of-phase"* combination of the d_{xy} Ru orbitals and the π system of the pyrazine. The corresponding doubly occupied bonding orbital is at lower energy and it is not shown in Figures 2 and 3. The other four d_π orbitals are nonbonding and form a packet of doubly occupied orbitals that lies between the SOMO and the LUMO (Figure 2), as already found with Xα-DVM calculations.[18] It should be noticed that the occupation of the β (or minority spin) orbitals follows a non-Fermi occupation scheme, independent of the functional used, as already observed,[18] other occupation schemes resulting in higher energies. The Fermi occupation scheme is recovered when using the **B2** basis, since the antibonding character of the $(d_\pi-\pi)$ interaction is enhanced.

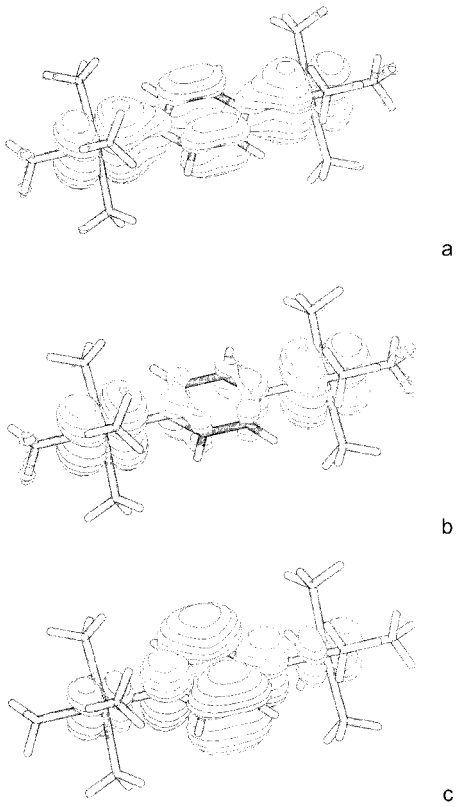

Figure 3. Isovalue representation of the ($d_\pi-\pi^*$) (a), ($d_\pi-\pi$)* (b), and ($d_\pi-\pi^*$)* (c) molecular orbitals of $[(NH_3)_5Ru(pyz)Ru(NH_3)_5]^{5+}$. The surfaces drawn correspond to $\Psi = 0.025(ea_0^{-3})^{1/2}$.

Table 3. Relevant Geometrical Parameters Computed for Pyrazine

ground state	LDA/Stoll	PW91	BP	MP2 [a]
N_p-C	1.3352	1.3383	1.3402	1.3477
CC	1.3928	1.3922	1.3936	1.3957
CN_pC	115.75	115.42	115.44	115.30
N_pCC	122.12	122.28	122.27	122.35

[a] Reference 43.

To better analyze the bonding interactions, we computed the structure of the free pyrazine ligand using LDA and GGA in C_{2v} symmetry. The relevant geometrical parameters obtained are reported in Table 3. In Table 3, we also report the geometrical parameters obtained through a MP2 approach[43] for the purpose of comparison with the DFT results. The agreement between the various methods is remarkable. Macroscopic evidence of the π-back-donation is the shortening of the C−C bond and the lengthening of the C−N_p bond computed when passing from the free ligand to the ligand inside the complex. From a comparison betweenthe C−C and C−N_p bonds reported in Tables 2 and 3, it can be noticed that the π-back-donation has a relatively small influence on the CC distance (maximum computed difference = 0.6%) and a greater effect on the C−N_p bond length (maximum computed difference = 1.8%).

Electronic Spectra. The electronic spectra of the $[(NH_3)_5Ru(pyz)Ru(NH_3)_5]^{5+}$ ion are characterized by three intense absorption bands centered at 6370, 17700, and 39700 cm^{-1}, respectively. These bands were assigned to the inter-valence (IT), metal-to-ligand charge transfer (MLCT) and $\pi-\pi^*$ pyrazine transition, respectively.[1] Using the orbital levels of Figure 2, these transitions correspond to the one-electron excitations ($d_\pi-\pi^*$) → ($d_\pi-\pi$)* for the IT transition and ($d_\pi-\pi$)* → ($d_\pi-\pi^*$)* for the MLCT transition. The $\pi-\pi^*$ transition is associated with the excitation from the $12b_2$ orbital (not shown in Figure 2) to the ($d_\pi-\pi^*$)* orbital. With this assignment, we computed the electronic spectrum using Slater's transition state method.[33] The influence of the geometry of the ion, of the functionals, and of the basis set on the transition energies was also explored by performing separate calculations using the optimized geometries and the X-ray structures, as well as the basis sets **B1** and **B2**, for several different functionals. The results of the calculations are summarized in Tables 4 and 5. As a general trend, we have noticed that the actual values of the computed transitions appear to be dependent on the functional used and on the basis set. Better agreement with the experimental data was obtained in any case using the X-ray structure especially for the IT and the MLCT transitions. Two different effects appear to influence the computed transitions: a direct effect due to the basis set and the exchange-correlation functional used, and an indirect effect due to the differences in the geometries optimized with the different functionals and basis set. The direct effect can be estimated from the calculation performed using the X-ray structure (Table 4), while both direct and indirect effects can be seen from the transition computed using the optimized geometries (Table 5). The direct effect of the functional is relatively small since the transitions computed with the X-ray structure are almost independent from the functional used within the same basis set (Table 4). The new basis set gave transitions at higher energies. The large difference between the transitions computed using the optimized geometries for the different functional can be therefore ascribed mainly to the geometrical (indirect) effect. It must be noticed that the $\pi-\pi^*$ transition is less sensitive to this effect. A general improvement of the IT energy was obtained using the **B2** basis set (Table 5). When using the optimized structure, the best agreement with the experimental spectra is obtained with the **B2** basis set and the GGA-relativistic approach.

Table 4. Electronic Transitions of the $[(NH_3)_5Ru(pyz)Ru(NH_3)_5]^{5+}$ Ion Computed on the Crystallographic Geometry[a]

basis B1	LDA/Stoll	PW91	BP	LDA/Rel	exptl[b]
IT	6904	6814	6812	7267	6370
MLCT	17604	17564	17530	17000	17700
$\pi-\pi^*$	36956	36090	36093	not converged	39700

basis B2	LDA/Stoll	PW91	BP	LDA/Rel	exptl[b]
IT	7699	7438	7444	8159	6370
MLCT	20533	20476	20506	19074	17700
$\pi-\pi^*$	not converged	36199	36152	37844	39700

[a] From ref 42. Scalar relativistic correction (Rel) included as described in the text. [b] From ref 1.

These findings are in line with the results that one could expect when comparing theoretical calculations performed in vacuo with experimental spectral data. It is, in fact, already well-known that Ru−pyrazine complexes undergo significant red-shift of the MLCT band as the solvent donor number (DN) increases.[29,30,44] Furthermore, the IT transition shows a blue-shift, although less pronounced, as the solvent DN increases. This shift becomes particularly evident upon crown ether

(43) Calculations performed with the Gaussian94 program package (6-31G basis set): Frish, M. J.; Trucks, G. W.; Schlegel, H. B.; Gill, P. M. W.; Johnson. B. G.; Robb, M. A.; Cheeseman, J. R.; Keith, T. A.; Petersson, G. A.; Montgomery, J. A.; Rsghavachari, K.; Al-Laham, M. A.; Zakrewski, V. G.; Ortiz, J. V.; Foresman, J. B.; Cioslowski, J.; Stefanov, B. B.; Nanayakkara, A.; Challacombe, M.; Peng, C. Y.; Ayala, P. Y.; Chen, W.; Wong, M. W.; Andres, J. L.; Replogle, E. S.; Gomperts, R.; Martin, R. L.; Fox, D. J.; Binkley, J. S.; DeFrees, D. J.; Baker, J.; Stewart, J. P.; Head-Gordon, M.; Gonzales, C.; Pople, J. A. *Gaussian 94*; Gaussian Inc.: Pittsburgh, PA, 1996.

(44) Creutz, C.; Chou, M. H. *Inorg. Chem.* **1987**, *26*, 2995.

Table 5. Electronic Transitions of the $[(NH_3)_5Ru(pyz)Ru(NH_3)_5]^{5+}$ Ion Computed on the Optimized Structures

basis B1	LDA/Stoll	PW91	BP	LDA/Rel[a]	exptl[b]
IT	4371	2919	3145	5105	6370
MLCT	20356	22010	22043	19527	17700
$\pi-\pi^*$	35980	33819	33625	36860	39700

basis B2	LDA	LDA/Stoll	PW91	BP	LDA/Rel[a]	PW91/Rel[a]	BP/Rel[a]	exptl[b]
IT	7025	6880	5606	5460	8332	8389	6670	6370
MLCT	23559	23269	23995	24027	21486	21624	21664	17700
$\pi-\pi^*$	37626	37093	34956	34641	38585	35970	35303	39700

[a] Scalar Relativistic Correction (Rel) included as described in the text. [b] From ref 1.

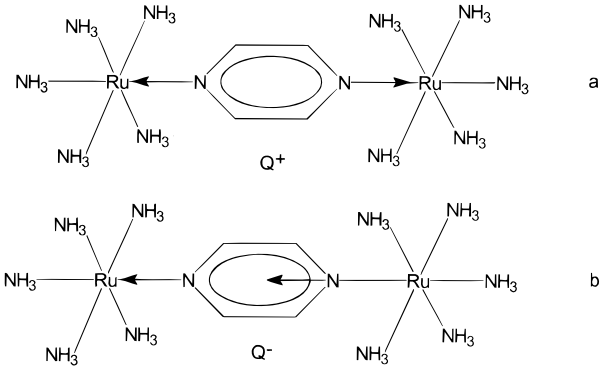

Figure 4. Schematic drawings of the nuclear displacements for the Q^+, symmetric, (a) and Q^-, antisymmetric, stretch (b) of the $Ru-N_p$ bonds.

encapsulation.[22,45] Since our calculations were performed in vacuo (DN = 0), we expect to find the MLCT at higher energy and the IT at lower energy than the experimental transition. Furthermore, the computed relative small shift of the IT with respect to the MLCT as a function of the different functionals (and therefore different optimized geometries) is in line with the observed shift ratio between the blue (IT) and red (MLCT) shifts as a function of the DN of the solvent.

Adiabatic Potential Surfaces. The ground state properties of mixed-valence systems depend on the vibronic coupling mechanism which determines the properties of the complexes. In particular, the extent of localization of the "extra" electron influences the form of the absorption bands. It seems experimentally well established that the Creutz−Taube salt is a completely electronically delocalized mixed-valence complex (Class III, according to the Robin and Day classification[46]). The modeling of valence trapping phenomena requires the knowledge of the potential energy surface of the system as a function of the position of the atomic nuclei. To this end we have performed calculations varying the $Ru-N_p$ bond distance from the equilibrium position, as determined by geometrical optimization, and optimizing all the rest of the molecule. In this way, we constructed adiabatic potential energy surfaces (PES). The $Ru-N_p$ distances were varied according to the nuclear displacements schematically shown in Figure 4 and the two sections of the PES reported in Figure 5 were computed. The molecular rearrangements following the modes shown in Figure 4 are completely negligible for all the NH_3 groups except for the axial ones. In particular, the maximum displacements for these axial ammonia molecules correspond to 0.03 and 0.05 Å for the modes shown in Figures 4a and 4b, respectively. Assuming that the $Ru-NH_3$ stretch is not coupled with the $Ru-N_p$ stretch, the two sections correspond respectively to a symmetric (Q^+, Figure 5a) and an antisymmetric (Q^-, Figure 5b) $Ru-N_p$ stretching. The effect of the exchange-correlation functional and of the basis set, as well as the influence of the relativistic correction, is shown in Figure 4b for Q^-. The Q^+ PES was computed using the model chemistry which led to the best optimized geometry (i.e. the PW91 nonlocal functional plus relativistic corrections using the **B2** basis set for Ru). The $Ru-N_p$ distances were kept constant at each point while all the remaining nuclear degrees of freedom were optimized. For the Q^- PES, the Ru−Ru distance was frozen at its equilibrium value, i.e. at the optimized value for the same model chemistry.

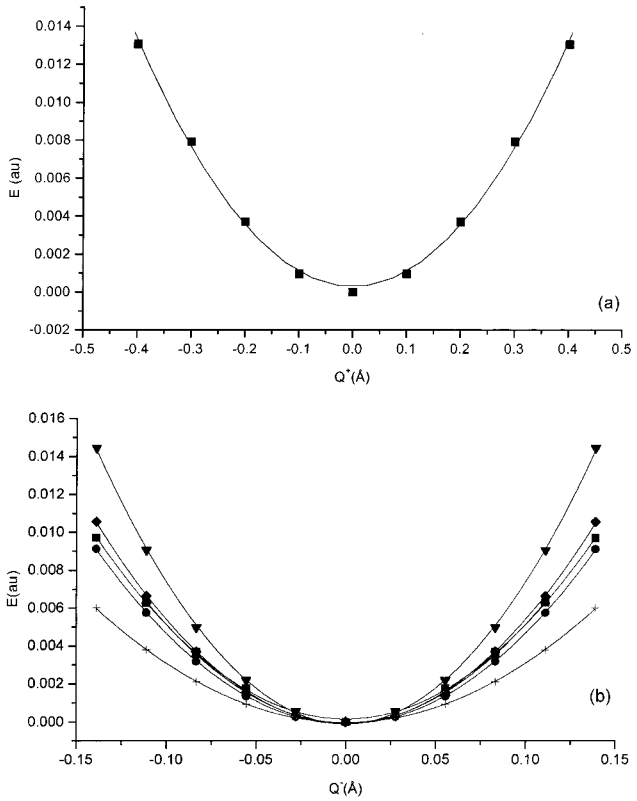

Figure 5. Computed potential energy surfaces for the symmetric (a) and antisymmetric stretch (b) of the $Ru-N_p$ bonds. The displacement with respect to the equilibrium distance is in angstroms and all the energies are rescaled to the energy of the optimized one (in the same model chemistry). (a) ● LDA nonrelativistic; (b) ■ PW91, ● BP, ▲ BP relativistic, ▼ LDA relativistic, ◆ PW91 relativistic; + LDA (**B1**).

The PES sections present a single minimum and this is a theoretical confirmation that the Creutz−Taube ion indeed can be classified as a Class III[46] mixed-valence compound. From the computed PES sections it is also possible to estimate the frequency of the Ru−pyz local bond vibration. This quantity is useful in the construction of vibronic model Hamiltonians, like those of refs 17, 21, and 23, which can be used to calculate the line shape profile of the near-IR−vis bands. We can compute

(45) Hupp, J. T.; Dong, Y. *Inorg. Chem.* **1994**, *33*, 4421.
(46) Robin, M. B.; Day, P.; Burgi, H. B. *Adv. Inorg. Chem. RadioChem.* **1967**, *10*, 247.

Table 6. Computed Frequencies[a] (cm^{-1}) for the Q^+ and Q^- Normal Modes for $[(NH_3)_5Ru(pyz)Ru(NH_3)_5]^{5+}$

Q^-	ω_a[d]	Q^-	ω_a[d]
LDA[b]	266(5)	PW91	368(17)
LDA[c]	424(7)	BP[c]	357(28)
BP	328 (15)	PW91[c]	359(10)
Q^+	ω_s[d]		
PW91[c]	139(1)		

[a] Calculations performed using the **B2** basis set, if not explicitly mentioned. Experimental frequencies were found at 334 and 326 cm^{-1}, as discussed in the text. [b] **B1** basis set. [c] Scalar relativistic correction included as described in the text. [d] Deviation from harmonic behavior in parentheses.

this value by a proper analysis of the potential energy curves. In particular, computation of the distance, in mass weighted coordinates, between structures built by linear synchronous transit or constrained optimization leads to an effective one-dimensional Schrödinger equation for the motion of a particle with a unitary mass.[47] This equation can be numerically solved to obtain anharmonic frequencies for this motion as fully implemented in the program package DiNa.[48] The results of this analysis are reported in Table 6. The computed anharmonicity of the two coordinates is small (less than 8% in the worst case, BP) and we can therefore consider, with a good approximation, that in the energy range considered the two modes are harmonic. These two vibrational modes, which are totally symmetric in C_s, can be labeled in the idealized C_{2v} symmetry as antisymmetric, ω_a, and symmetric, ω_s, respectively. The value of the antisymmetric stretching frequency, ω_a, does not strongly depend on the functional used, the largest difference being between the LDA and GGA results. When comparing only the results for nonlocal functionals, the computed values of ω_a are within 10%, including both relativistic and nonrelativistic corrections. Since the PW91 functional with relativistic correction affords the best geometrical parameters for the ground state (Table 2), we used this functional to compute the symmetric (ω_s) Ru−N_p stretching frequency, which resulted in $\omega_s = 139$ cm^{-1}.

Since the actual geometry of the ion, both in crystal and in solution, is lower than C_{2v} due to local distortion, both the above modes should be Raman active. The Raman experiments by Hupp et al.[13] showed, below 400 cm^{-1}, two peaks at 334 and 326 cm^{-1}, respectively assigned as Ru−NH_3 and Ru−N_p stretch (in ref 13b slightly lower values, 262 and 324 cm^{-1}, respectively, were reported). The computed Ru−N_p stretch ($\omega_a = 359$ cm^{-1} for relativistic PW91) is in nice agreement with the experimental value ($\omega_a = 326$ cm^{-1}). The lowest stretching at around 139 cm^{-1} was not observed.

From the frequencies of the two normal modes it is possible to estimate the frequency of the local Ru−N_p stretching vibration (ω_l), performing a normal-to-local mode transformation. This can be easily accomplished, when looking at the Creutz−Taube ion as an A−B−A molecule, with the bending angle fixed at 180°, assuming that the two local vibrations are not coupled.[49] Thus we get:

$$\omega_s = \omega_l\sqrt{\frac{m_2}{m_1 + m_2}}$$

$$\omega_a = \omega_l\sqrt{\frac{2m_1 + m_2}{m_1 + m_2}} \qquad (1)$$

where m_1 is the mass of the $Ru(NH_3)_5$ fragment and m_2 is that of the pyrazine. Using eq 1 and ω_A and ω_S from Table 6, we obtained values of ω_l between 275 and 254 cm^{-1}. We suggest using values of ω_l within this range in vibronic model Hamiltonians which include the Ru−pyz bond vibration.

Conclusions

Density functional theory has been successfully applied to characterize the electronic structure of the Creutz−Taube mixed-valence dinuclear complex ion $[(NH_3)_5Ru\text{-}pyz\text{-}Ru(NH_3)_5]^{+5}$ with an analysis of the ground-state potential energy surface to confirm the classification of the complex as a Class III mixed-valence compound.

Since, in DFT the choice of the functional plays a major role in comparing results of the calculation with experimental data, we have compared the results obtained with several functionals when computing the geometry of the complex as well as on the computed electronic and vibronic coupling. The best geometry was obtained with a modified basis set for Ru and using the nonlocal PW91 functional with relativistic corrections. From the present calculations we can also conclude that the rather large variability in the computed electronic spectrum has to be ascribed mainly to geometrical (indirect) effects, which can contribute to the observed dependence of the electronic spectra in solution upon the particular solvent used in the experiment.

The computed adiabatic potential energy surfaces were harmonic (to a good approximation) with frequencies, for the symmetric and antisymmetric Ru−pyrazine strecthing modes, of 139 and 359 cm^{-1}, respectively. The last value agrees well with the experimental value of 326 cm^{-1}. The localized Ru−N_p vibration in the range 254−275 cm^{-1} can be associated with these stretching frequencies and should be used in future model Hamiltonians which aim to include the Ru−pyz bond vibration to describe the spectral features of the Creutz−Taube ion.

This is an example of the ability of DFT to give information not only on the spectroscopic and magnetic properties of large chemical systems, such as polynuclear transition metal complexes, but also on the PES of the system. DFT seems to offer a unique tool to handle the localization−delocalization of electrons in mixed-valence systems and therefore we expect that this approach can play an interesting role in characterizing electron-transfer systems. A more accurate study of the potential energy surface would require calculations along coordinates other than Q^+ and Q^-. This could give more insight into the phenomenon of electron delocalization and should provide crucial information on the vibrations active in the electron transfer process. It is still a matter of some debate to assess the relative importance of the Ru−ammonia, Ru−pyrazine, and pyrazine stretchings in determining the IT and MLCT line shape profiles observed for the Creutz−Taube salt. This point cannot be addressed in the present article since a much more extensive analysis of the PES is required. Due to the complexity of the molecular system, this interesting problem is hard to tackle and the calculations are extremely time consuming. We hope, however, to be able to address this problem soon.

Acknowledgment. Thanks are expressed to Prof. Enzo Benedetti from the Dipartimento di Chimica e Chimica Industriale, Universita′ di Pisa for valuable and fruitful discussions.

(47) Barone, V.; Minichino, C. *Theochem* **1995**, *330*, 325.
(48) DiNa Program, Release 2.1, by V. Barone, University of Naples.
(49) (a) Herzberg, G. *Infrared and Raman Spectra of Polyatomic Molecules*; Van Nostrand: Toronto, Canada, 1945; p 172. (b) Steinfield, J. I. *Molecules and Radiation*; Harper & Row: New York, 1974; p 181.

This work was supported by the Swiss National Foundation and the COST Action D9.

Supporting Information Available: The **B2** basis, in the format of an atomic data set for ADF2.3 (Table SI) (PDF). This material is available free of charge via the Internet at http://pubs.acs.org.

JA9920258